Impaired neurogenesis and synaptogenesis in iPSC-derived Parkinson's patient cortical neurons with D620N VPS35 mutation

Ute Scheller[1,2], ChoongKu Lee[2], Philip Seibler[3], Miso Mitkovski[4], JeongSeop Rhee[2 #], Christoph van Riesen[1,5 #]

[1] Department of Neurology, University Medical Center Göttingen, Germany

[2] Department of Molecular Neurobiology, Synapse Physiology Group, Max Planck Institute of Multidisciplinary Sciences, Göttingen, Germany

[3] Institute of Neurogenetics, University of Lübeck, Germany

[4] City Campus Light Microscopy Facility, Max Planck Institute of Multidisciplinary Sciences, Göttingen, Germany

[5] German Center for Neurodegenerative Diseases (DZNE), Göttingen, Germany

[#]corresponding author

Dr. Christoph van Riesen, Dept. of Neurology, University Medical Center Göttingen, Robert-Koch-Str. 40, 37075 Göttingen, Germany, phone: +495513962184, fax: +49551398405, christoph.van-riesen@med.uni-goettingen.de

Dr. JeongSeop Rhee, Department of Molecular Neurobiology, Synaptic Physiology Group, Max Planck-Institute for Multidisciplinary Sciences, Herrmann-Rein-Str. 3, 37075 Göttingen, Germany, phone: +4955120131694, rhee@mpinat.mpg.

Running Title:

Synaptic dysfunction in VPS35 Parkinson's disease

Abstract

Presynaptic dysfunction is an important early process in the pathophysiology of Parkinson´s disease (PD) that drives disease progression. To gain insight into the intrinsic synapse impairment in PD, we performed comprehensive electrophysiological and morphological analysis of iPSC-derived cortical neurons derived from PD patients with the VPS35-D620N mutation. Our findings reveal significant impairment in neurogenesis and synaptogenesis within individual patient neurons, culminating to synaptic dysfunction even in the absence of neuronal interactions. The neurons exhibited significantly reduced synaptic responsiveness, fewer synapse and decreased dendritic length and complexity. Thus, the VPS35-D620N mutation in human cortical neurons independently can cause pathophysiology via synaptic dysfunction. Our study highlights the urgent need to develop disease-modifying therapies aimed at preserving synaptic function in PD.

Introduction

Parkinson´s disease (PD) is the second most common neurodegenerative disease after Alzheimer´s disease[1]. Recent cumulative evidence suggests that the pathophysiology of PD is initiated and driven by presynaptic mechanisms. This notion is supported by the fact that in post-mortem studies in human patients, 90% of aggregated alpha-synuclein is located presynaptically[2,3]. The neurodegenerative process is thought to start at the level of the synapse and then spread more proximally to the soma[4]. Imaging studies in early PD patients have shown a reduction in presynaptic markers, particularly in the substantia nigra pars compacta (SNpc) and dopamine transporter in the striatum suggesting that presynaptic pathology may precede dopaminergic cell death[5,6]. Aberrant cortico-striatal activity and degeneration of cortico-striatal glutamatergic synapses have been proposed as independent stressors for dopaminergic neurons in the SN, suggesting at least some disease propagation from the cortex downwards[7,8]. Cortico-striatal and nigrostriatal terminals form a highly interactive complex with medium spiny neurons (MSNs) in the striatum. It has been argued that the focal symptom onset of PD reflects the somatotopic organization of the cortex and the striatum and is therefore better explained by an early cortical input-driven pathology than by random dopaminergic degeneration in the non-somatotopically organized SNpc[7]. In addition, transcranial magnetic stimulation (TMS) has demonstrated that alterations in cortical plasticity and cortical disinhibition occur at an early stage in PD, representing either a compensatory or a maladaptive change that contributes to disease progression[9–11]. Dopaminergic neurons have been described as particularly vulnerable due to cell-autonomous factors, including their high arborization with long axons, high firing rate with broad spikes and slow Ca^{2+}-oscillations among others[12], which may contribute to the neurodegeneration in complex PD pathophysiological changes. Dysfunction of the cortical input onto the basal ganglia system may be an additional stressor leading to dopaminergic degeneration in PD.

Despite the recent insights into the importance of presynaptic mechanisms in the pathophysiology of PD, there questions remain many unanswered. The lack of animal models for sporadic PD has slowed progress in this field. Consequently, animal models carrying monogenic mutations that lead to PD in humans are of significant value. Monogenic mutations have been identified in 10% of PD patients[1], including a rare pathogenic autosomal dominant variant D620N in the vacuolar sorting protein 35 (VPS35)[13,14]. Patients with VPS35 mutations develop late-onset levodopa-responsive parkinsonism that is clinically indistinguishable from sporadic PD[15]. The precise mechanism by which VPS35 mutations, including the D620N mutation, cause degeneration of the nigrostriatal dopamine and other neurotransmitter systems in humans remains elusive[16], largely due to a paucity of comprehensive data on their impact on neuronal function. VPS35 is part of the retromer complex, which is involved in the endosomal transport system[16,17]. The VPS35-D620N mutation has been described to affect endosomal-lysosomal pathways[18], impair mitochondrial function[19], and to be associated with synaptic dysfunction[16]. VPS35 is part of the retromer complex, which is involved in the endosomal transport system[16,17]. The VPS35-D620N mutation has been described to affect endosomal-lysosomal pathways[18], impair mitochondrial function[19], and to be associated with synaptic dysfunction[16].

This study aimed to further elucidate the role of VPS35 in human PD, with a particular focus on synaptic mechanisms. We used an autaptic neuronal culture system to enable the detailed study of the intrinsic electrophysiological and morphological properties of iPSC-derived VPS35 D620N cortical single neurons from PD patients. In the absence of any external stimuli, we observed that neurogenesis (dendritic complexity and length), synaptogenesis and synaptic strength were impaired in the patient-derived cell lines. These unique properties of each mutant neuron have the potential to significantly impact the neuronal network in PD, thereby highlighting their importance in causing synaptic pathology.

Methods

Cell lines

The iPSC lines have been characterized previously and were derived from dermal fibroblasts of two healthy donors (SFC086-03-01, C1; SFC084-03-02, C2) and two Parkinson's disease patients (iPS-L6731-7, PD1; iPS-L6634-5, PD2) carrying a heterozygous c.1858G>A (p.D620N) missense mutation in the *VPS35* gene (Supplementary Table S1). The cell lines are abbreviated from here on as C1, C2, PD1 and PD2, respectively. After the completion of the experiments in our lab, routine karyotypic analysis of the iPSC cultures in another laboratory revealed chromosomal abnormalities in the C2 control line after long-term passaging (SFC084-03-02: 46,XX,del(10)(p12p12)[15]/45,idem,-X[5]). As our experiments had already been completed and no cells were left, we were unable to determine whether the C2 cells used carried the karyotypic change.

All participants provided written informed consent (Ethics Committee that approved this part of the study: University of Lübeck, Lübeck, Germany). All iPSC lines were cultured on Matrigel (BD Bioscience) coated dishes in mTeSR1 medium (STEMCELL Technologies).

Differentiation into cortical neurons

The direct differentiation of iPSCs into cortical neurons was performed as previously described [20,21]. Briefly, iPSCs were dissociated into single cells using Accutase (Life Technologies) and replated onto Matrigel-coated dishes. Differentiation was initiated by adding the SMAD pathway inhibitors dorsomorphine (Tocris; 1µM) and SB 431542 (Tocris; 10µM) to the cultures. From day 13 to 17, the cells were cultured in neural maintenance medium (NMM)[20] containing basic fibroblast growth factor (R&D Systems; 20ng/ml) and brain-derived neurotrophic factor (BDNF, STEMCELL Technologies; 20ng/ml). Neural rosettes were replated on day 18 in NMM with BDNF, glial cell-derived neurotrophic factor (GDNF,

STEMCELL Technologies; 20ng/ml), and ascorbic acid (Sigma-Aldrich; 0.2mM). The medium was changed every other day until day 27. On day 28, the rosettes were dissociated using Accutase and plated in NMM supplemented with BDNF, GDNF, and ascorbic acid. The medium was replaced every 2-3 days until day 43. On day 43, BDNF, GDNF, and ascorbic acid were removed, and the cells were cultured in NMM until day 44//49.

Cell Culture

Human iPSC (hiPSC) were seeded onto prepared mouse astrocyte feeder cells according to previously established protocols[22]. Briefly, mouse astrocytes were obtained from dissected cortex of P0 wild-type animals, enzymatically digested with trypsin-EDTA and cultured in DMEM (GIBCO) for 7-10 days. 6-well culture plates with coverslips were prepared to allow the growth of astrocyte micro-islands. Glass coverslips were coated with agarose and stamped with a customized stamp to generate islands coated with poly-D-lysine, acetic acid and collagen[23]. hIPS were thawed in a water bath at 37°C, diluted in an iPS medium containing ROCK inhibitor (48% DMEM/F12, 48% Neurobasal medium, 1% N2, 1% B27, 0.1% beta-mercaptoethanol, 0.5% L-glutamine, 0.5% NEAA, 0.5% FBS, 0.1% ROCK inhibitor), filtered through a 40µm cell strainer (BD Falcon) and counted using tryptan blue staining. Appropriate numbers of cells were seeded onto the prepared astrocyte microislands and incubated at 37°C for 24 hours. The complete iPS-medium was replaced with fresh medium without ROCK inhibitor the next day and changed once per week for the following culture period. hiPSCs were seeded onto prepared mouse astrocyte feeder cells according to previously established protocols[22]. Briefly, mouse astrocytes were obtained from dissected cortex of P0 wild-type animals, enzymatically digested with trypsin-EDTA and cultured in DMEM (GIBCO) for 7-10 days. 6-well culture plates with coverslips were prepared to allow the growth of astrocyte micro-islands. Glass coverslips were coated with agarose and stamped with a customized stamp to generate islands coated with poly-D-lysine, acetic acid and collagen[23]. hIPS were thawed in

a water bath at 37°C, diluted in an iPS medium containing ROCK inhibitor (48% DMEM/F12, 48% Neurobasal medium, 1% N2, 1% B27, 0.1% beta-mercaptoethanol, 0.5% L-glutamine, 0.5% NEAA, 0.5% FBS, 0.1% ROCK inhibitor), filtered through a 40µm cell strainer (BD Falcon) and counted using tryptan blue staining. Appropriate numbers of cells were seeded onto the prepared astrocyte microislands and incubated at 37°C for 24 hours. The complete iPS-medium was replaced with fresh medium without ROCK inhibitor the next day and changed once a week for the following culture period.

Electrophysiology

Autaptic neurons were whole-cell patch clamped either using either a Multiclamp 700B (Axon Instruments, Molecular Devices) or an EPSC10 (HEKA electronics) amplifier controlled by Clampex software (Axon Instruments, Molecular Devices) or Patchmaster 2 (HEKA electronics), respectively. The extracellular bath solution (140mM NaCl, 4mM CaCl2, 4mM KCl, 10mM HEPES, 24mM MgCl2, 10mM glucose, adjusted to pH 7.3, and ~310msOsmol/l) was maintained at a constant flow and pharmacological solutions were added as required using a custom-made flow pipette. Glass pipettes were made using a Sutter 2000 filament-based horizontal puller and their resistance ranged between 2.5 and 3.5 MΩ. The patch pipette solution consisted of 136 mM KCl, 17.8 mM HEPES, 1 mM EGTA, 4.6 mM MgCl2, 4 mM NaATP, 0.3 mM Na2GTP, 15 mM creatine phosphate, and 5 U/ml phosphocreatine kinase (315-320 mOsmol/l), pH 7.4. Neurons were visualized using an inverted microscope (Zeiss or Olympus). Only neurons with series resistance <15MΩ were analysed. For voltage clamp recordings cells were held at -70mV. In voltage mode synaptic responses and voltage-gated channel currents were evoked by electrical stimuli with a frequency of 0.2Hz and a stepwise (10mV) increase in membrane holding potentials from -80 to +70mV for 500ms each. To block glutamatergic and GABAergic receptors 10µM NBXQ (HelloBio) and 10µM bicuculline (Tocris) were added to the extracellular solution using a flow pipette aimed at the cell and the combined voltage-gated

sodium and potassium channel current (I_{total}) was measured. To isolate I_K, 300nM TTX (Tocris) was applied exogenously and then 1mM 4-AP was added to record I_{DR}. I_{Na} was calculated by subtracting I_K from I_{total} and A-type I_K (I_A) was calculated by subtracting I_{DR} from I_K. The densities of all currents were normalized to cell capacitance (pF). Using the current clamp mode R_{input} was calculated from membrane potential chance by current injection from -100pA to 0pA in 20pA intervals for 1s each. Action potentials (AP) were evoked by stepwise increasing (+10pA) current injection starting from 0pA. The patch pipette solution used to record these membrane properties consisted in 138mM K-gluconate, 16.8mM HEPES, 10mM NaCl, 1 mM $MgCl_2$ 6H2O, 0.25mM EGTA, 4mM ATP-Mg^{2+}, 0.3mM GTP–Na^+ (solution adjusted to pH 7.4, 320mOsmol/litre). All experiments were performed at room temperature. All recordings were analyzed using AxographX software (version 1.5.4., Axograph Scientific).

Immunofluorescence staining and imaging

Human autaptic neurons were washed with PBS, fixed with 4%PFA for 15 min, washed with PBS, quenched with 50mM glycine for 10 min, washed again with PBS and incubated with iT-FX image enhancer (Life Technologies) for 30 min. Cells were then permeabilized with 0.1% Triton X-100/2.5% NGS/PBS for 40 min, blocked with 2.5% NGS/PBS and incubated with primary antibodies for 1 hour. The primary antibodies used were: MAP2 (chicken, 1:1000, Novus Biological), SHANK2 (guinea pig, 1:250, Synaptic Systems), Synapsin 1/2 (rabbit, 1:500, Synaptic Systems). Cells were washed with 0.1% Triton X-100/2.5% NGS/PBS and incubated with secondary antibodies for 45 min. The following secondary antibodies were used: Alexa Flour 405 (anti-chicken 1:1000, Abcam), Alexa Flour 488 (anti-guinea pig 1:1000, Thermo Fisher), Alexa Flour 568 (anti-rabbit 1:1000, Thermo Fisher). After a final wash with 0.1% Triton X-100/2.5% NGS/PBS and PBS, cells were mounted with Aqua-Poly Mount (Polyscience). All steps were carried at room temperature. Fluorescence images were captured using a Leica TCS SP8 X confocal laser scanning microscope (Leica Microsystems).

Image processing

Overlapping z-stacks (x,y,z: 229, 229, 299 nm) were acquired with the inverted Leica TCS SP8 X confocal laser scanning microscope equipped with a white light laser, motorized stage and a 63x 1.4 NA oil immersion objective. The Napari v. 0.4.18[24] Noise2Void plugin[25] was used to train a denoising model which was then applied to the corresponding channels of the original confocal images. For quality control purposes, the denoised channels were then merged with the original channels, reconstructed and calibrated using a custom written FIJI[26] macro and then converted using the Imaris File Converter (v. 10.1.0). The Imaris image visualization and analysis software package (v. 10.1.0) was used for image analysis. Synapses were counted by colocalization between pre- and postsynaptic puncta labelled by Synapsin 1/2 and Shank2 respectively. Puncta were also required to colocalize with MAP2 dendritic staining. The Imaris plugin Filament-tracer was used in a semi-automatic mode to detect the dendritic tree marked by MAP2 staining and to calculate the total dendrite length (sum), the number of dendritic branching points and Sholl intersections (Sholl analysis).

Statistical analysis

Statistical analysis and visualization were performed using GraphPad Prism (version 10.2.2, GraphPad Software). Data were checked for normality and, in the case of non-normal distribution, logarithmized (ln) prior to further analysis. To account for the factors ‘group’ (control vs PD), ‘subgroup’ (C1, C2, PD1, PD2) and ‘time’ (week 2-6), 3-way ANOVA was used to calculate differences between groups ‘control’ and ’PD’. Additional subgroup comparisons were made using 2-way ANOVA and supplemented by Tukey’s test for multiple comparisons. There was no significant interaction between ‘subject’ and ‘time’ for any of the parameters analyzed. Group data are presented as mean ± SEM or median (IQR) for non-parametric data respectively. For visualization purposes, group comparisons (PD vs control) are presented as box plots (Tukey), where the means (or medians respectively) of the time points

for each subgroup were calculated first, followed by the medians of the time points per group. Similarly, for subject comparisons, means or medians of time points were calculated first and presented as box plots (Tukey). All subgroup comparisons are shown in Supplementary Figures and Supplementary Table 3. Statistical results presented in box plots were calculated using 3-way or 2-way ANOVA. The significance level was set at $p<0.05$ (*≤0.05, **≤0.01, ***≤0.001, ****≤0.0001).

Results

In this study, two neuronal cell lines derived from two PD patients carrying the VPS35 D620N mutation were compared with two cell lines from controls. Direct differentiation of iPSCs into cortical glutamatergic neurons was performed as previously described[20,21]. For the analysis, the human neurons were seeded into an autaptic culture system, in which single neurons were placed on individual mouse astrocyte feeder islands. The autaptic culture system allows reproducible characterization of single hiPSC derived neurons, as we and others have recently demonstrated[22,27]. Our analysis included electrophysiological patch-clamp recordings and morphological analysis by immunocytochemistry imaging over a period of 6 weeks.

Neuronal differentiation and growth: active and passive membrane properties

First, we used whole-cell voltage and current patch-clamp recordings to measure passive and active membrane properties to verify proper neuronal development. Neuronal differentiation of hiPSCs could be demonstrated by typical morphological and membrane properties from 2 weeks in vitro (WIV) counted starting from the day of cultivation in the autaptic culture system.

Passive membrane properties

Measurements of passive membrane properties (capacitance, resting membrane potential (RMP) and input resistance (R_{input})) were used as parameters for cell development. Capacitance, as a measure of cell size, remained stable over 6 WIV (Fig 1a, Supplementary Table 2) and there was no statistical difference between PD and control neurons (Fig. 1b). RMP and R_{input} as markers for cell excitability decreased slightly but not significantly over time indicating cell maturation (Fig. 1c, e, Supplementary Table 2). Control cell lines had a significantly lower RMP than PD patient cell lines (p=0.0119, Fig. 1d, Supplementary Table 2) with C1 being hyperpolarized (subgroup analysis, Supplementary Table 3, Supplementary Fig. 1b). R_{input}

showed no significant difference between the VPS35-D620N patient and control cells (Fig. 1f, Supplementary Table 2).

Active membrane properties: Voltage-gated sodium and potassium channels

Next, we characterized active membrane properties by analyzing ion channel activity and action potential (AP) generation. First, we assessed the activity and density of voltage-gated sodium channels. The peak I_{Na} densities of PD and control neurons were identical (Fig. 2c, Supplementary Table 2). Similarly, the densities of I_K, delayed rectifier K^+-currents (I_{DR}) and fast transient A-type K^+-currents (I_A) were not different between PD and control groups (Fig. 2f, i, l, Supplementary Table 2). Although I_{Na} and I_A densities were statistically different over time ('time' factor: p=0.0428, p=0.0028, Supplementary Table 2), there was no clear developmental pattern (Fig. 2b, e, h, k).

Active membrane properties: action potentials

The hiPSC-derived neurons, which contained properly functioning voltage-gated ion channels, were found to generate AP. We characterized the APs by amplitude, duration, half-width, threshold, overshoot, afterhyperpolarisation (AHP), rheobase and firing pattern. The hiPSC-derived neurons were only analyzed, if normal ion channel function could be demonstrated. Six different AP firing patterns could be distinguished: abortive, immature, spontaneous, tonic, phasic I and phasic II (Supplementary Fig. 3a). To compare the numbers of APs, we selected the highest number from each cell recording. At the group level, PD neurons generated a significantly higher number of APs compared to controls (Fig. 3b). This effect was likely due to a decrease in the number of APs at WIV 5 and 6, predominantly in controls, which was reflected in a higher proportion of phasic I and absent tonic firing cells (Fig. 3a, Supplementary Fig. 3b, c, Supplementary Table 2). Control C1 also showed more phasic II and less spontaneous and tonic firing overall which might have further increased the difference (Supplementary Fig. 3b, Supplementary Table 2). No significant differences were found

between PD and control cell lines for rheobase, AP threshold, AP overshoot, AP amplitude, AP duration and AP half-width (Fig. 3d, f, h, j, l, n, Supplementary Table 2). The AHP amplitude was significantly smaller in PD neurons (p=0.0279, Fig. 3p, Supplementary Table 2). The different AP parameters remained stable over time in both groups (Fig. 3c, i, k, m, o), except for the AP threshold and AP overshoot which decreased slightly over time ('time' factor: p<0.0001, p=0.0044, Fig. 3e, g, Supplementary Table 2). AP duration and half-width decreased minimally but not significantly indicating further AP maturation (Fig. 3k, m).

Overall, the neurons matured by 2 WIV with little further growth thereafter. Active and passive membrane properties indicated proper neuronal differentiation in all cell lines with only minor differences between PD and control cells.

Impairment of synaptic release in PD neurons

We recorded evoked postsynaptic currents (eEPSC) to assess the development of functional synapses. The patient hiPSCs were significantly less likely to develop synaptic responses than those derived from controls (p<0.0001, Fig. 4c, Supplementary Table 2). In both groups the percentage of cells with a synaptic response increased over time ('time' factor: p=0.0043, Fig. 4b, Supplementary Table 2). While control neurons reached a steady state at 4 WIV, PD neurons showed a much slower increase. At 6 WIV, 65% and 69% of control cells developed a synaptic response whereas only 50% and 43% of PD cells did so. Further analysis of the subgroups (C1, C2, PD1, PD2) showed that the synaptic response was lower in each PD subject compared to each control (Supplementary Fig. 5a, Supplementary Table 3). In addition, EPSC amplitudes were significantly lower in PD neurons (p<0.0001, Fig. 4f, Supplementary Table 2). There was no significant change in EPSC amplitude over time (Fig. 4e). Each control subject had higher EPSC amplitudes than PD patient cells (Supplementary Fig. 5b, Supplementary Table 3). Thus, PD neurons were less likely to form functional synapses and had smaller eEPSC amplitudes than controls.

Morphological analysis: filament tracing and synapse counting

We used immunocytochemistry to monitor neurogenesis and synaptogenesis. Dendritic length and complexity were analyzed by MAP2 staining (filament tracing, Sholl analysis). In general, cells showed some diversity in morphological shape, with no marked differences between groups and time points (Fig. 5c). When comparing the two groups, it was found that control neurons had a greater total summed dendrite length than PD cells (p=0.0014, Fig. 5b, Supplementary Table 2). To varying degrees, the dendrite length tended to increase over time in all groups up to 5 weeks ('time' factor, p=0.0013, Fig. 5a, Supplementary Table. 2). To examine the dendritic complexity, we analyzed the number of dendritic branching points and Sholl intersections. While the number of dendritic branching points did not differ between groups (Fig. 5e, Supplementary Table 2), the number of Sholl intersections was significantly reduced in PD neurons compared to controls, indicating a higher complexity of the control cell lines (p=0.0006, Fig. 5h, Supplementary Table 2). The number of dendritic branching points increased by 3 weeks and fluctuated by 6 WIV, while the dendritic length increased up to 5 WIV ('time' factor p=0.0105, p=0.0043, Fig. 5d, g, Supplementary Table. 2).

Next, we wanted to investigate whether the reduced synaptic response rate was due to reduced synaptogenesis in general or due to a reduced number of functional synapses. We analyzed colocalized pre- and postsynaptic puncta labelled with the presynaptic marker Synapsin 1/2 and the postsynaptic marker Shank2, to identify them as synapses (Fig. 6c, d). The PD groups showed a significant decrease in the total number of synapses compared to the control neurons (p<0.0001, Fig. 6b, Supplementary Table 2). In addition, there were significant differences in number of synapses during neuronal development. In the control neurons, the number of synapses increased significantly up to WIV 4 and then decreased slightly at WIV 6 ('time' factor p=0.0003, Fig. 6a, Supplementary Table 2). In the PD groups, however, there were no obvious changes in synapse numbers from week to week. There was a clear dissociation

316 between the rate of neuronal development and the rate of new synapse formation ('time' factor
317 p=0.0003, Fig. 6a, Supplementary Table 2). Subgroup comparisons confirmed significant
318 differences between all control and PD cell lines (Supplementary Fig. 5c, Supplementary Table
319 3).

320 In conclusion, our study demonstrated significant impairments in neurogenesis, marked by
321 reduced dendritic length and complexity, and in synaptogenesis, indicated by a decreased
322 number of synapses and functional synapses, in hiPSC-derived neurons from PD patients with
323 the D620N VPS35 mutation compared to controls.

324

Discussion

Modelling an age-related human neurodegenerative disease such as PD presents numerous challenges. To address this, we utilized human cortical iPSC-derived neurons from two PD patients carrying the VPS35 D620N mutation as a simplified cellular model and monitored them for six weeks. To date, only a few electrophysiological studies of human, predominantly dopaminergic iPSC-derived neurons from PD patients, have been conducted using large-scale culture systems. However, these culture systems present a challenge in distinguishing whether observed phenotypes are due to the neurons themselves or from interactions with neighboring neurons. The autaptic culture system excludes inter-neuronal communication, thus allowing us to focus exclusively on the intrinsic properties of the targeted neurons. As a result, the phenotypes observed in VPS35 D620N hiPSC-derived neurons were not influenced by extraneous factors such as dopaminergic stimulation or environmental fluctuations, rendering them invaluable for elucidating the aberrant neuronal network characteristic of Parkinson's patients.

Growth pattern

The control cell line C2 developed a karyotypic change (46,XX,del(10)(p12p12)[15]/45,idem,-X[5]) after long-term passaging. Although there is some heterogeneity between the control groups in terms of membrane properties and morphological shape, we did not observe any significant difference between them in general. Furthermore, heterogeneity in cellular iPSC-derived models is a well-known issue, which emphasizes the importance of using multiple, or in the best case, isogenic controls[28].

Impaired neurogenesis

Given that VPS35 plays a key role within the retromer complex, which is critical for endosomal protein sorting and intracellular transport[16,17], it is plausible to hypothesize that the VPS35-

D620N mutation potentially contributes to Parkinson's disease through various disruptive cellular mechanisms. The mutation has been associated with impaired neurogenesis[29–31]. The published phenotypic manifestations of the D620N VPS35 mutation in the literature so far such as dopaminergic cell death[29,30], reduced neuronal proliferation, neurite degeneration, impaired neurite outgrowth and dendritic complexity[31], show some variability and remain inconclusive. For example, one study investigating the effect of the PD-associated VPS35 mutation on dopaminergic hiPSC-derived neurons revealed reduced differentiation efficiency and increased apoptosis compared to controls[29], whereas in another study human dopaminergic neurons derived from PD patients with the VPS35 mutation differentiated into dopaminergic neurons similar to controls[32]. Inconsistencies have also been observed in VPS35-D620N knock-in mouse models (VKI). While Chen et al. observed degeneration of dopaminergic neurons and neurites in certain brain regions (animals aged 13 months)[30], others found no such degeneration or changes in younger animals (aged 3 months) or in primary cortical cell cultures from VKI mice (DIV 21)[33,34]. This variability may be influenced by experimental models and conditions, and the timing of assessments, amongst others. Highlighting the importance of long-term observations to detect age-related phenotypes consistent with the delayed dopaminergic degeneration observed in PD patients, a recent study found dopaminergic cell loss and elevated dopamine levels only in older animals (aged 15/16 months) but not before[35].

Beyond the dopaminergic system, a recent study examined neurogenesis in the hippocampal neural progenitor pool of transgenic mice carrying the VPS35-D620N mutation[31]. The study unveiled a diminished pool of neural progenitors, alongside reduced proliferation and migration, coupled with impaired neurite outgrowth characterized by diminished length and complexity in hippocampal neurons, signifying impaired neurogenesis[31]. Similar morphological changes have been observed in neurons derived from PD patients with other genetic mutations, including diminished neurite length and complexity in IPSC-derived cells

harboring Parkin and LRRK2 mutations, as well as reduced soma size and neuronal extensions in cells from idiopathic PD patients[36–40].

In our study, we found that human cortical iPSC-derived neurons with the VPS35-D620N mutation also showed impaired neurogenesis, characterized by reduced dendritic length and cell complexity.

These findings suggest that impaired neurogenesis may represent a general PD phenotype, that extends beyond dopaminergic cells. Further investigation is essential to unravel the contributions of these pathways to neurodegeneration and to elucidate the neurogenesis deficits seen in cellular models of PD.

Impaired synaptogenesis and reduced number of functional synapses

The presence of VPS35 at synapses underscores its significance in synaptic function[41,42]. Numerous studies have explored synaptic dysfunction in VPS35-deficient models, with a particular focus on cortical and dopaminergic neurons of animal models. This research has identified changes in synapse quantity[41,43], spine formation[43], synaptic vesicle dynamics[43,44], neurotransmitter release[33,45] and clustering and surface expression of AMPA receptors[41,43], indicating a broad association of VPS35 with various synaptic functions. However, the findings relating to synaptic morphology and vesicle number have been inconsistent, potentially due to differences in experimental models (animal, KD, VKI), conditions (large-scale culture), and timing of assessments[33,34,42]. At the single cell level, our findings revealed significantly lower proportions of neurons with a synaptic response, reduced EPSC amplitudes and fewer synapses in IPSC-derived cortical neurons from PD patients carrying the VPS35 D620N mutation, suggesting impaired synaptogenesis in human VPS36 D620N cell lines.

Previous studies have not demonstrated a clear correlation between changes in synapse numbers and mEPSC size[34,41,43]. In our investigation, spanning from WIV 2 to 6, we observed that while synapse numbers in control neurons increased steadily in tandem with neuronal development,

399 the EPSC size remained relatively stable, with only a slight increase at WIV 6. This indicates
400 that despite an increase in synaptic formation during neuronal maturation, the absolute number
401 of functional synapses remained largely unchanged. However, after 6 weeks, a reduction in
402 synapse numbers paradoxically corresponded with an increase in the absolute number of
403 functional synapses, leading to an enhanced EPSC size. It is likely that the period between WIV
404 2 and 6 is critical for functional synaptic conversion during neuronal development, though such
405 conversion also occurs even when synapse numbers were lower. In D620N VPS35 mutants, the
406 number of synapses fluctuated slightly over time but remained relatively stable with a small
407 increase at week 6. Correspondingly, EPSC amplitudes showed fewer fluctuations than controls.
408 Overall, PD patient-derived neurons showed a decrease in the total number of synapses and a
409 reduction in neurons with synaptic responses compared to control, highlighting a significant
410 impairment in synaptic function.
411 Therefore, we speculate that the abnormalities in synaptogenesis caused by D620N VPS35
412 mutants not only disrupt synapse formation but also selectively impair the conversion of
413 structural synapses into functional ones. Consequently, PD-derived neurons exhibit not only a
414 reduced number of synapses but also a diminished rate of functional synapse conversion.
415 The underlying molecular mechanisms of these synaptic anomalies likely involve disruptions
416 in endosomal trafficking[46]. In particularly, VPS35 has been associated with early and late
417 endosomes[47], which are essential for synaptic vesicle recycling[48] and AMPA receptor
418 trafficking[49]. In human dopaminergic iPSC-derived neurons carrying the VPS35 D620N
419 mutation, VPS35 co-localised with Rab5 and Rab7, markers of early and late endosomes, and
420 showed reduced velocity and lower fission- and fusion-frequency of Rab5- and Rab7-vesicles
421 compared to controls[29]. Thus, impaired trafficking of endocytosed SV could lead to an
422 abnormal vesicle pool and altered expression of neurotransmitter receptors on plasma
423 membranes, resulting in synaptic dysfunction. Our data in D620N mutant neurons suggest that
424 VPS35 influences the formation of individual synapses and is differentially involved in the

establishment of functional synapses in each neuron. However, the precise mechanisms by which the VPS35 mutation affects synaptogenesis, resulting in reduced synapse numbers and synaptic dysfunction, remains to be fully elucidated.

Moreover, synaptic dysfunction has also been implicated in other PD genes, including SNCA, LRRK2, Parkin and PINK1 amongst others[8,50–53]. For example, significantly reduced synaptic vesicle density was found in IPSC-derived dopaminergic neurons from a PD patient with a LRRK2 mutation[54]. However, data on synaptic transmission in IPSC derived PD neurons are scarce and show incongruent changes of sEPCS[55,56]. Furthermore, genome-wide studies in PD have identified differentially expressed genes associated with mitochondrial functions and protein degradation but also with synaptic vesicle dynamics and synaptic transmission[57,58]. This broader involvement of synaptic dysfunction underscores its pivotal role in the pathophysiology of PD, potentially even preceding dopaminergic neurodegeneration, as suggested by early imaging studies[5,6].

Conclusion

In conclusion, we have identified, for the first time, impaired neurogenesis and synaptogenesis in human glutamatergic iPSC-derived neurons from PD patients with the VPS35-D620N mutation. This discovery establishes a definitive synaptic phenotype in cortical neurons in a human-derived PD model. To uncover the precise mechanisms behind impaired neurite outgrowth and synaptic dysfunction, further research should investigate the synaptic vesicle pool, synaptic plasticity, and postsynaptic receptor density in greater detail. . The establishment of robust in vitro PD models is hampered by the complex nature of the basal ganglia, a critical structure in PD pathophysiology, comprising various interacting cell types, nuclei, input- and output structures. Although our single-cell model is by default oversimplified, our results support the emerging notion of early presynaptic dysfunction beyond just dopaminergic neurons in PD. Enhancing our understanding of PD pathomechanisms and developing valid

450 models for pharmacological testing are essential for enabling potential new treatments.
451 Continued research is crucial to deepen our understanding of PD pathomechanisms and explore
452 possible interventions.

453

Acknowledgment

We thank Anja Günther for her excellent technical support during experiments and Albrecht Sigler for his expertise and excellent support during imaging analysis. US was funded by a scholarship from the Deutsche Forschungsgemeinschaft (DFG, German Research Foundation) - 413501650.

Authors contribution

JSR, CvR, US conceived study and designed experiments. PS generated and provided human iPSC-derived neurons. US, CKL performed experiments. US, CKL, MM analysed data. JSR, CvR and US wrote the paper. All authors were involved final editing of the paper.

Conflict of interest

The authors declare that they have no conflict of interest.

References

1. Lau LML De, Breteler MMB. Epidemiology of Parkinson ' s disease. 2006;5(June):525-535.

2. Kramer ML, Schulz-Schaeffer WJ. Presynaptic α-synuclein aggregates, not Lewy bodies, cause neurodegeneration in dementia with lewy bodies. *J Neurosci*. 2007;27(6):1405-1410. doi:10.1523/JNEUROSCI.4564-06.2007

3. Schulz-Schaeffer WJ. The synaptic pathology of α-synuclein aggregation in dementia with Lewy bodies, Parkinson's disease and Parkinson's disease dementia. *Acta Neuropathol*. 2010;120(2):131-143. doi:10.1007/s00401-010-0711-0

4. Orimo S, Uchihara T, Nakamura A, et al. Axonal α-synuclein aggregates herald centripetal degeneration of cardiac sympathetic nerve in Parkinson's disease. *Brain*. 2008;131(3):642-650. doi:10.1093/brain/awm302

5. Matuskey D, Tinaz S, Wilcox KC, et al. Synaptic Changes in Parkinson Disease Assessed with in vivo Imaging. *Ann Neurol*. 2020;87(3):329-338. doi:10.1002/ana.25682

6. Delva A, Van Weehaeghe D, Koole M, Van Laere K, Vandenberghe W. Loss of Presynaptic Terminal Integrity in the Substantia Nigra in Early Parkinson's Disease. *Mov Disord*. 2020;35(11):1977-1986. doi:10.1002/mds.28216

7. Foffani G, Obeso JA. A Cortical Pathogenic Theory of Parkinson's Disease. *Neuron*. 2018;99(6):1116-1128. doi:10.1016/j.neuron.2018.07.028

8. Gcwensa NZ, Russell DL, Cowell RM, Volpicelli-Daley LA. Molecular Mechanisms Underlying Synaptic and Axon Degeneration in Parkinson's Disease. *Front Cell Neurosci*. 2021;15. doi:10.3389/fncel.2021.626128

9. Ammann C, Dileone M, Pagge C, et al. Cortical disinhibition in Parkinson's disease. *Brain*. 2021;143(11):3408-3421. doi:10.1093/BRAIN/AWAA274

10. Kojovic M, Bologna M, Kassavetis P, et al. Functional reorganization of sensorimotor cortex in early Parkinson disease. *Neurology*. 2012;78(18):1441-1448. doi:10.1212/WNL.0b013e318253d5dd

11. Kojovic M, Kassavetis P, Bologna M, et al. Transcranial magnetic stimulation follow-up study in early Parkinson's disease: A decline in compensation with disease progression? *Mov Disord*. 2015;30(8):1098-1106. doi:10.1002/mds.26167

12. Surmeier DJ, Obeso JA, Halliday GM. Selective neuronal vulnerability in Parkinson disease. *Nat Rev Neurosci*. 2017;18(2):101-113. doi:10.1038/nrn.2016.178

13. Kumar KR, Weissbach A, Heldmann M, et al. Frequency of the D620N mutation in VPS35 in Parkinson disease. *Arch Neurol*. 2012;69(10):1360-1364. doi:10.1001/archneurol.2011.3367

14. Deutschländer A, Ross OA, Wszolek ZK. VPS35 -Related Parkinson Disease Summary Genetic counseling. 2019:1-17.

15. Zimprich A, Benet-Pagès A, Struhal W, et al. A mutation in VPS35, encoding a subunit of the retromer complex, causes late-onset parkinson disease. *Am J Hum Genet*. 2011;89(1):168-175. doi:10.1016/j.ajhg.2011.06.008

16. Sassone J, Reale C, Dati G, Regoni M, Pellecchia MT, Garavaglia B. The Role of VPS35 in the Pathobiology of Parkinson's Disease. *Cell Mol Neurobiol*. 2021;41(2):199-227. doi:10.1007/S10571-020-00849-8

17. Brodin L, Shupliakov O. Retromer in Synaptic Function and Pathology. *Front Synaptic Neurosci*. 2018;10. doi:10.3389/fnsyn.2018.00037

18. Tang FL, Liu W, Hu JX, et al. VPS35 Deficiency or Mutation Causes Dopaminergic Neuronal Loss by Impairing Mitochondrial Fusion and Function. *Cell Rep*. 2015;12(10):1631-1643. doi:10.1016/j.celrep.2015.08.001

19. Wang W, Wang X, Fujioka H, et al. Parkinson's disease-associated mutant VPS35 causes mitochondrial dysfunction by recycling DLP1 complexes. *Nat Med*. 2016;22(1):54-63. doi:10.1038/nm.3983

20. Shi Y, Kirwan P, Livesey FJ. Directed differentiation of human pluripotent stem cells to cerebral cortex neurons and neural networks. *Nat Protoc*. 2012;7(10):1836-1846. doi:10.1038/nprot.2012.116

21. Grütz K, Seibler P, Weissbach A, et al. Faithful SGCE imprinting in iPSC-derived cortical neurons: An endogenous cellular model of myoclonus-dystonia. *Sci Rep*. 2017;7. doi:10.1038/srep41156

22. Rhee HJ, Shaib AH, Rehbach K, et al. An Autaptic Culture System for Standardized Analyses of iPSC-Derived Human Neurons. *Cell Rep*. 2019;27(7):2212-2228.e7. doi:10.1016/j.celrep.2019.04.059

23. Burgalossi A, Jung SY, Man K nok M, et al. Analysis of neurotransmitter release mechanisms by photolysis of caged Ca2+ in an autaptic neuron culture system. *Nat Protoc*. 2012;7(7):1351-1365. doi:10.1038/nprot.2012.074

24. Ahlers J, Althviz Moré D, Amsalem O, et al. napari: a multi-dimensional image viewer for Python. July 2023. doi:10.5281/zenodo.8115575

25. Krull A. Noise2Void. *Cvpr*. 2019;2019-April:502-506.

26. Schindelin J, Arganda-Carreras I, Frise E, et al. Fiji: An open-source platform for biological-image analysis. *Nat Methods*. 2012;9(7):676-682. doi:10.1038/nmeth.2019

538 27. Fenske P, Grauel MK, Brockmann MM, Dorrn AL, Trimbuch T, Rosenmund C.
539 Autaptic cultures of human induced neurons as a versatile platform for studying
540 synaptic function and neuronal morphology. *Sci Rep*. 2019;9(1):1-12.
541 doi:10.1038/s41598-019-41259-1

542 28. Volpato V, Webber C. Addressing variability in iPSC-derived models of human
543 disease: Guidelines to promote reproducibility. *DMM Dis Model Mech*. 2020;13(1).
544 doi:10.1242/dmm.042317

545 29. Bono K, Hara-Miyauchi C, Sumi S, Oka H, Iguchi Y, Okano HJ. Endosomal
546 dysfunction in iPSC-derived neural cells from Parkinson's disease patients with VPS35
547 D620N. *Mol Brain*. 2020;13(1). doi:10.1186/s13041-020-00675-5

548 30. Chen X, Kordich JK, Williams ET, et al. Parkinson's disease-linked D620N VPS35
549 knockin mice manifest tau neuropathology and dopaminergic neurodegeneration. *Proc*
550 *Natl Acad Sci U S A*. 2019;116(12):5765-5774. doi:10.1073/pnas.1814909116

551 31. Jiang M, Tu HT, Zhang K, et al. Impaired neurogenesis in the hippocampus of an adult
552 VPS35 mutant mouse model of Parkinson's disease through interaction with APP.
553 *Neurobiol Dis*. 2021;153:105313. doi:10.1016/J.NBD.2021.105313

554 32. Hanss Z, Larsen SB, Antony P, et al. Mitochondrial and Clearance Impairment in
555 p.D620N VPS35 Patient-Derived Neurons. *Mov Disord*. 2021;36(3):704-715.
556 doi:10.1002/mds.28365

557 33. Cataldi S, Follett J, Fox JD, et al. Altered dopamine release and monoamine
558 transporters in Vps35 p.D620N knock-in mice. *npj Park Dis*. 2018;4(1).
559 doi:10.1038/s41531-018-0063-3

560 34. Kadgien CA, Kamesh A, Milnerwood AJ. Endosomal traffic and glutamate synapse
561 activity are increased in VPS35 D620N mutant knock-in mouse neurons, and resistant

to LRRK2 kinase inhibition. *Mol Brain*. 2021;14(1). doi:10.1186/S13041-021-00848-W

35. Niu M, Zhao F, Bondelid K, et al. VPS35 D620N knockin mice recapitulate cardinal features of Parkinson's disease. *Aging Cell*. 2021;20(5). doi:10.1111/ACEL.13347

36. Corenblum MJ, McRobbie-Johnson A, Carruth E, et al. Parallel neurodegenerative phenotypes in sporadic Parkinson's disease fibroblasts and midbrain dopamine neurons. *Prog Neurobiol*. 2023;229(June):102501. doi:10.1016/j.pneurobio.2023.102501

37. MacLeod D, Dowman J, Hammond R, Leete T, Inoue K, Abeliovich A. The Familial Parkinsonism Gene LRRK2 Regulates Neurite Process Morphology. *Neuron*. 2006;52(4):587-593. doi:10.1016/J.NEURON.2006.10.008

38. Pu J, Gao T, Zheng R, et al. Parkin mutation decreases neurite complexity and maturation in neurons derived from human fibroblasts. *Brain Res Bull*. 2020;159:9-15. doi:10.1016/j.brainresbull.2020.03.006

39. Ren Y, Jiang H, Hu Z, et al. Parkin mutations reduce the complexity of neuronal processes in iPSC-derived human neurons. *Stem Cells*. 2015;33(1):68-78. doi:10.1002/stem.1854

40. Sánchez-Danés A, Richaud-Patin Y, Carballo-Carbajal I, et al. Disease-specific phenotypes in dopamine neurons from human iPS-based models of genetic and sporadic Parkinson's disease. *EMBO Mol Med*. 2012;4(5):380-395. doi:10.1002/emmm.201200215

41. Munsie LN, Milnerwood AJ, Seibler P, et al. Retromer-dependent neurotransmitter receptor trafficking to synapses is altered by the Parkinson's disease VPS35 mutation p.D620N. *Hum Mol Genet*. 2015;24(6):1691-1703. doi:10.1093/hmg/ddu582

586 42. Vazquez-Sanchez S, Bobeldijk S, Dekker MP, Van Keimpema L, Van Weering JRT.
587 VPS35 depletion does not impair presynaptic structure and function. *Sci Rep*.
588 2018;8(1). doi:10.1038/s41598-018-20448-4

589 43. Tian Y, Tang FL, Sun XD, et al. VPS35-deficiency results in an impaired AMPA
590 receptor trafficking and decreased dendritic spine maturation. *Mol Brain*. 2015;8(1).
591 doi:10.1186/s13041-015-0156-4

592 44. Inoshita T, Arano T, Hosaka Y, et al. Vps35 in cooperation with LRRK2 regulates
593 synaptic vesicle endocytosis through the endosomal pathway in Drosophila. *Hum Mol*
594 *Genet*. 2017;26(15):2933-2948. doi:10.1093/hmg/ddx179

595 45. Ishizu N, Yui D, Hebisawa A, et al. Impaired striatal dopamine release in homozygous
596 Vps35 D620 N knock-in mice. *Hum Mol Genet*. 2016;25(20):4507-4517.
597 doi:10.1093/hmg/ddw279

598 46. Williams ET, Chen X, Otero PA, Moore DJ. Understanding the contributions of VPS35
599 and the retromer in neurodegenerative disease. *Neurobiol Dis*. 2022;170.
600 doi:10.1016/J.NBD.2022.105768

601 47. Rojas R, Van Vlijmen T, Mardones GA, et al. Regulation of retromer recruitment to
602 endosomes by sequential action of Rab5 and Rab7. *J Cell Biol*. 2008;183(3):513-526.
603 doi:10.1083/jcb.200804048

604 48. Granseth B, Odermatt B, Royle SJJ, Lagnado L. Clathrin-Mediated Endocytosis Is the
605 Dominant Mechanism of Vesicle Retrieval at Hippocampal Synapses. *Neuron*.
606 2006;51(6):773-786. doi:10.1016/j.neuron.2006.08.029

607 49. Hausser A, Schlett K. Coordination of AMPA receptor trafficking by Rab GTPases.
608 *Small GTPases*. 2019;10(6):419-432. doi:10.1080/21541248.2017.1337546

609 50. Lee W, Koh S, Hwang S, Kim SH. Presynaptic dysfunction by familial factors in

610 Parkinson disease. *Int Neurourol J*. 2018;22(Suppl 3):S115-S121.
611 doi:10.5213/inj.1836216.108

612 51. Ebanks K, Lewis PA, Bandopadhyay R. Vesicular Dysfunction and the Pathogenesis of
613 Parkinson's Disease: Clues From Genetic Studies. *Front Neurosci*. 2020;13.
614 doi:10.3389/fnins.2019.01381

615 52. Pischedda F, Piccoli G. LRRK2 at the pre-synaptic site: A 16-years perspective. *J*
616 *Neurochem*. 2021;157(2):297-311. doi:10.1111/jnc.15240

617 53. Skelton PD, Tokars V, Parisiadou L. LRRK2 at Striatal Synapses: Cell-Type
618 Specificity and Mechanistic Insights. *Cells*. 2022;11(1). doi:10.3390/cells11010169

619 54. Nguyen M, Krainc D. LRRK2 phosphorylation of auxilin mediates synaptic defects in
620 dopaminergic neurons from patients with Parkinson's disease. *Proc Natl Acad Sci U S*
621 *A*. 2018;115(21):5576-5581. doi:10.1073/pnas.1717590115

622 55. Stern S, Lau S, Manole A, et al. Reduced synaptic activity and dysregulated
623 extracellular matrix pathways in midbrain neurons from Parkinson's disease patients.
624 *npj Park Dis*. 2022;8(1). doi:10.1038/s41531-022-00366-z

625 56. Kouroupi G, Taoufik E, Vlachos IS, et al. Defective synaptic connectivity and axonal
626 neuropathology in a human iPSC-based model of familial Parkinson's disease. *Proc*
627 *Natl Acad Sci U S A*. 2017;114(18):E3679-E3688. doi:10.1073/pnas.1617259114

628 57. Huang J, Liu L, Qin L, Huang H, Li X. Weighted Gene Coexpression Network
629 Analysis Uncovers Critical Genes and Pathways for Multiple Brain Regions in
630 Parkinson's Disease. *Biomed Res Int*. 2021;2021. doi:10.1155/2021/6616434

631 58. Borrageiro G, Haylett W, Seedat S, Kuivaniemi H, Bardien S. A review of genome-
632 wide transcriptomics studies in Parkinson's disease. *Eur J Neurosci*. 2018;47(1):1-16.
633 doi:10.1111/ejn.13760

Figure 1

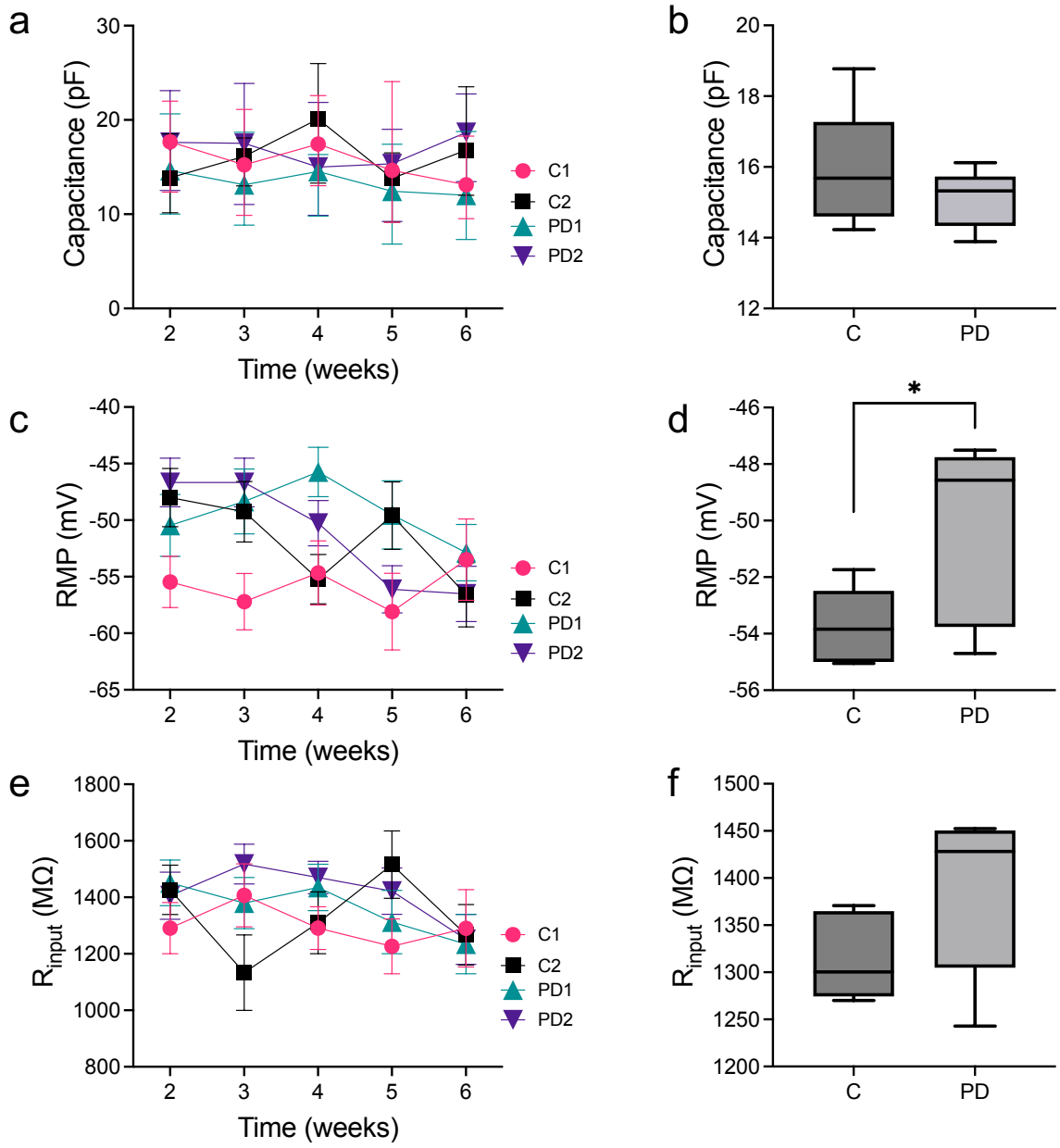

Figure 2

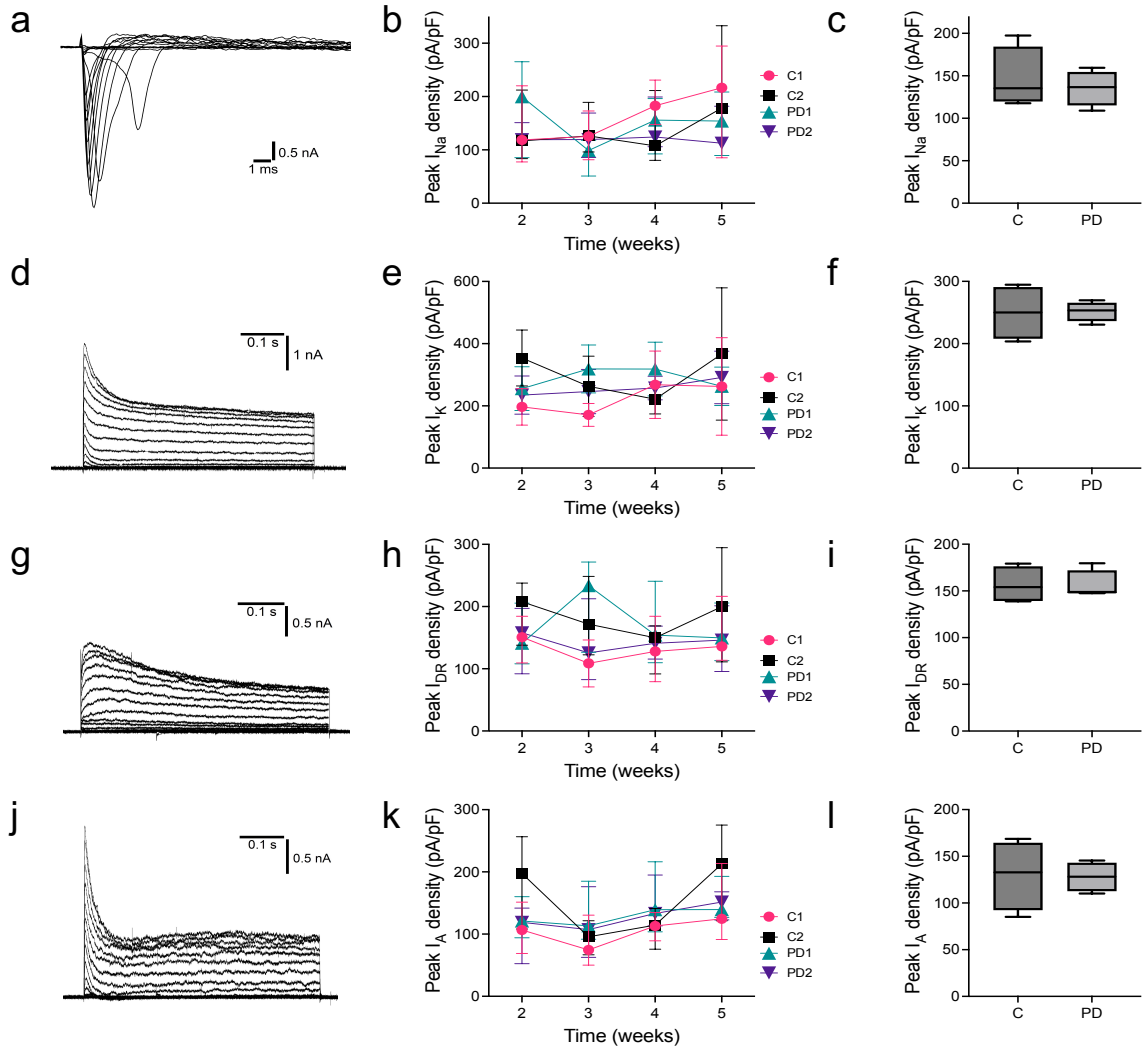

Figure 3

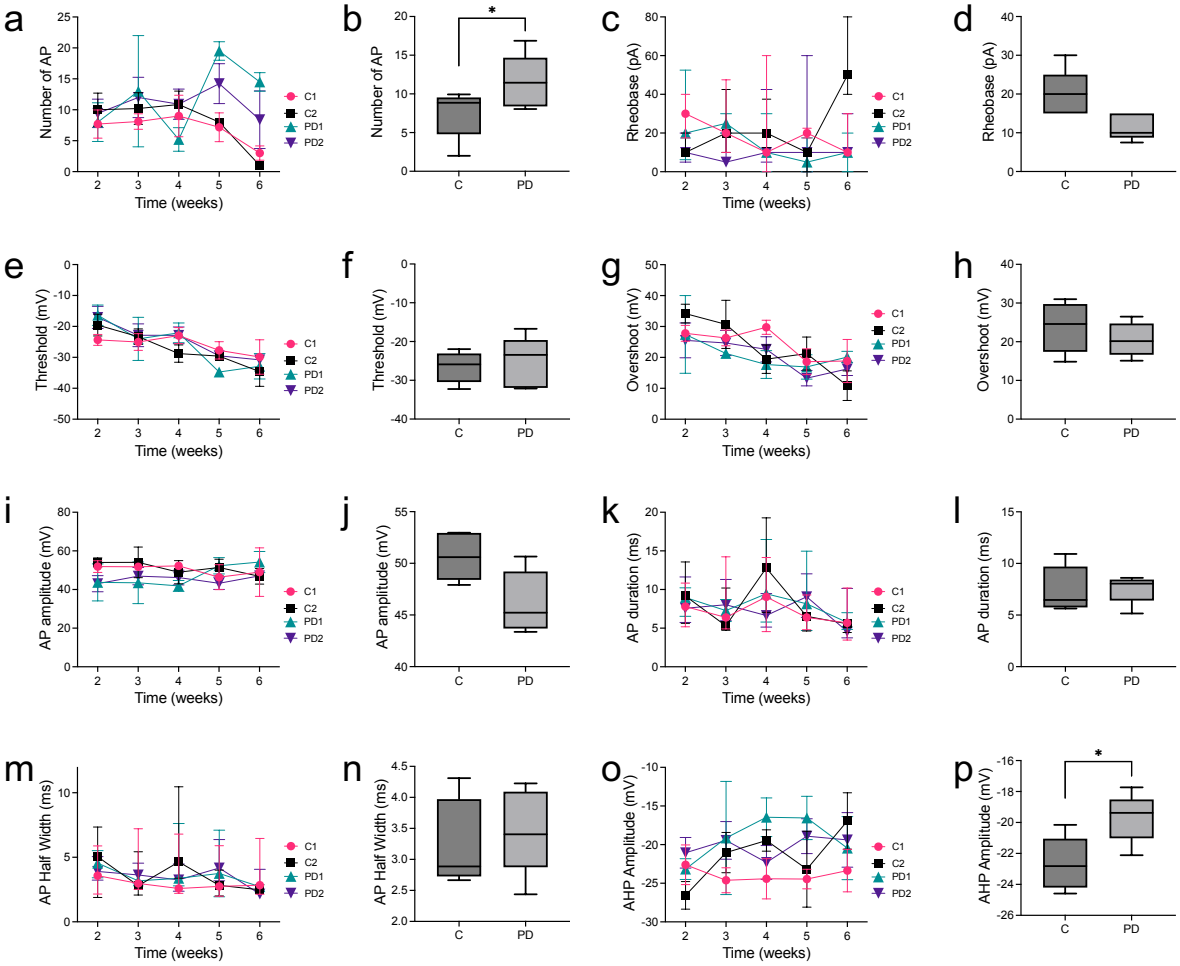

Figure 4

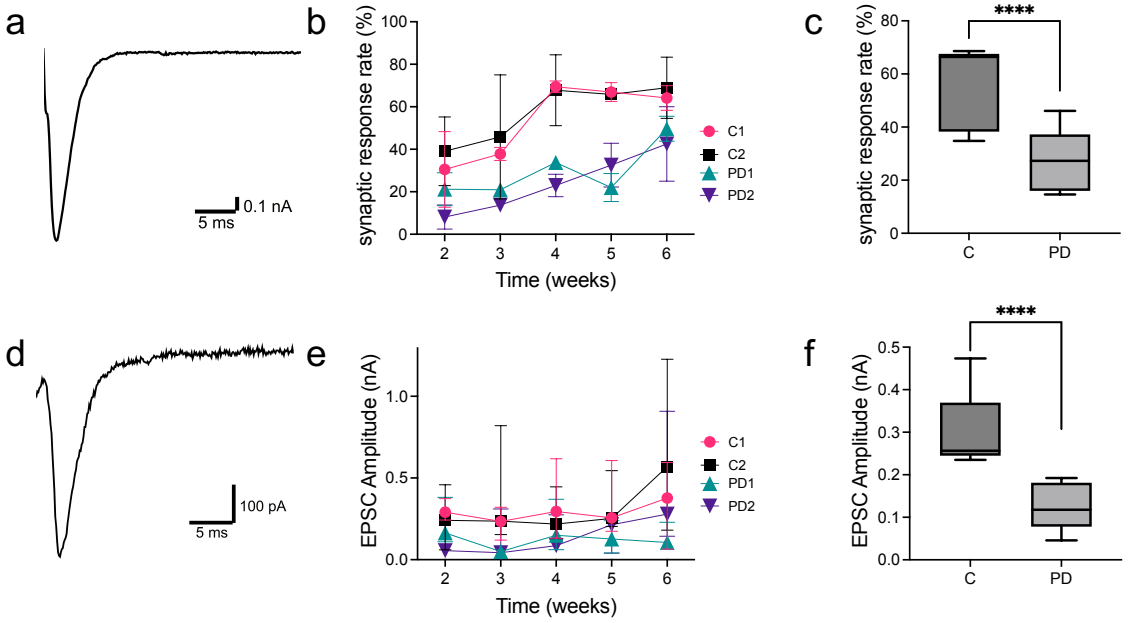

Figure 5

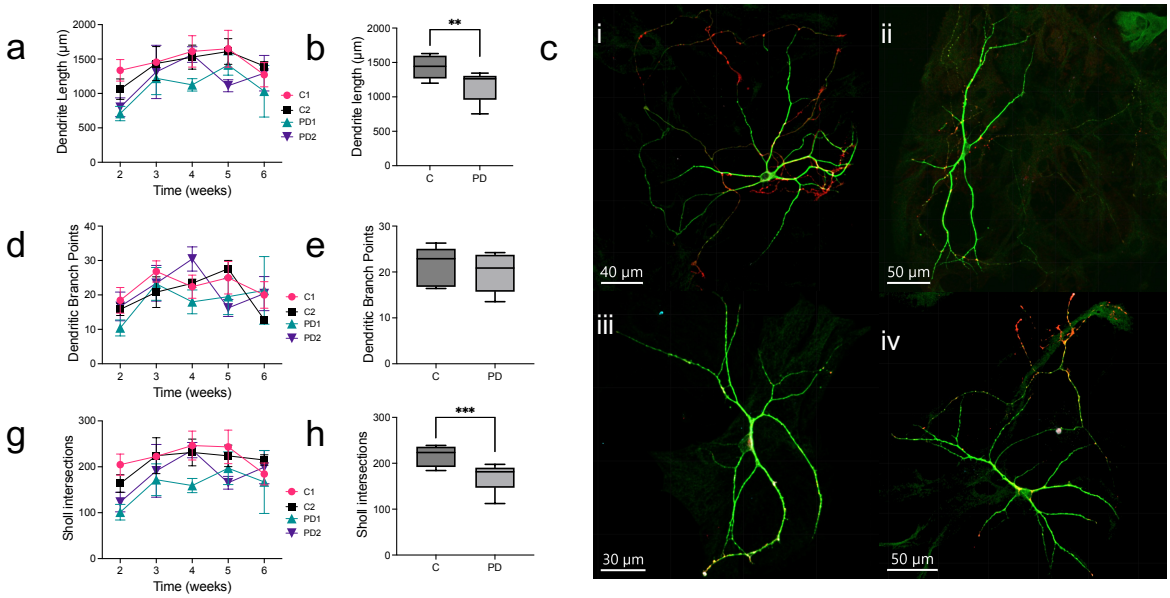

Figure 6

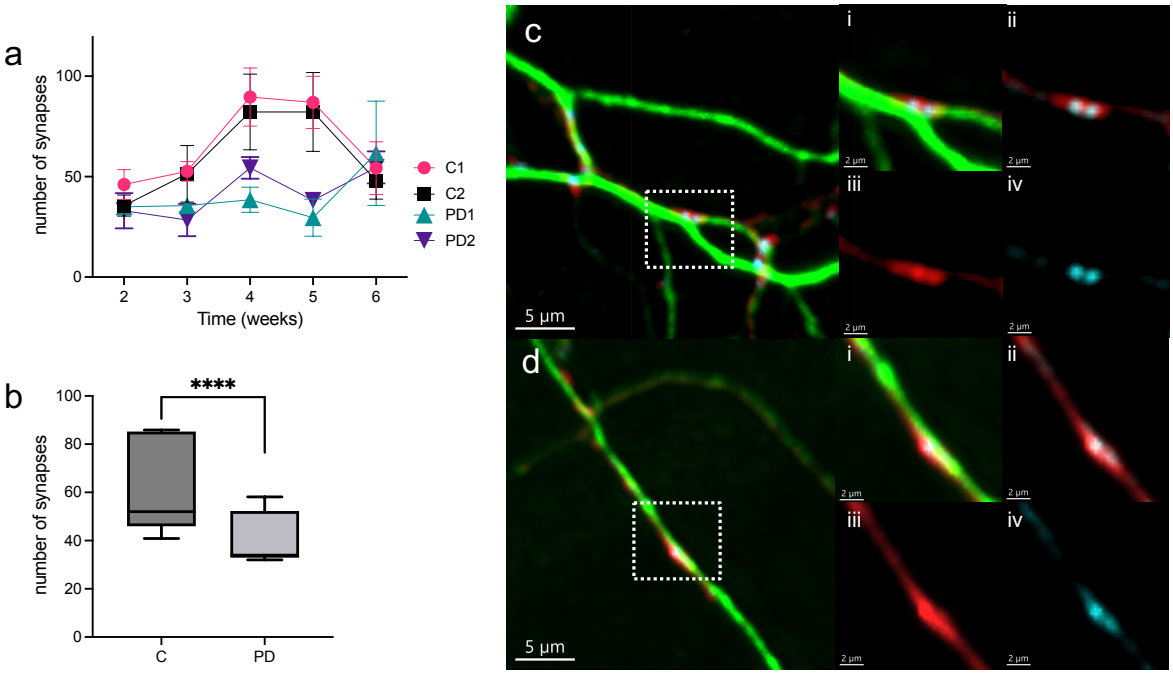

Figure legends

Figure 1. Passive Membrane Properties

(a) Cell capacitance for each subgroup and timepoint over 6 WID. Medians (IQR) are shown. (**b)** Group comparison of cell capacitance between control and PD cell-lines. (**c)** RMP for each subgroup over time. (**d**) Group comparison reveals controls had significantly lower RMP in control cell-lines. (**e)** Rinput per subgroup over time **d** and **f** group comparison between control vs PD. In graphs **c** and **e** means ± SEM are shown.

Figure 2. Voltage-gated Channels

Voltage-gated sodium and potassium currents are shown as peak current densities**. (a**, **d**, **g** and **j)** Representative traces showing depolarization-induced I_{Na}, I_K, I_{DR} and I_A, respectively. (**b**, **e**, **h**, and **k)** Peak current densities over time for each subgroup. For all graphs medians (IQR) are given. (**c**, **f**, **i**, and **l)** Group comparison of peak current densities control vs PD cell-lines.

Figure 3. Active Membrane Properties

Various parameters generating and shaping action potential (AP) are shown along with the iPSC-derived neuron development (**a, c, e, g, l, k, m, o**) and in group comparison (**b, d, f, h, j, l, n, p**). Peak AP-number (**a** and **b**), Rheobase (**c** and **d**), Threshold (**e** and **f**), Overshoot (**g** and **h**), AP amplitude (**i** and **j**), AP duration (**k** and **l**), AP half width (**m** and **n**) and AHP amplitude (**o** and **p**) over WID. In **a**, **k** and **m** median (IQR), in **c, e, g, i** and **o** means ±SEM are depicted.

Figure 4: Synaptic Response

(**a**, **d)** Representative traces of EPSC from control (**a**) and PD (**d**) neurons at 4 WID each. (**b** and **e**) The proportion of neurons synaptic release and EPSC amplitude over time. (**c** and **f**) Group comparisons for the proportion of neurons with synaptic release and EPSC amplitude control versus PD patient cell lines. In **e** median (IQR) and in **b** means ±SEM are given.

Figure 5. Morphological Analysis

(**a**, **d**, **g**) Dendritic filament length (sum), number of branching points and average numbers of dendrites intersecting Sholl circles up to 200 μm distance per subgroup over time. (**b, e, h**) Group comparison between control and PD patient cell-lines. (**c**) Representative fluorescence images for human autaptic neurons for each subgroup at 4 WID. **ci** and **cii** are control neurons and **ciii** and **civ** are neurons induced from PD cell-lines. For immunohistochemical staining, MAP2 (green) was used as dendritic, Synapsin1/2 (red) as presynaptic and Shank2 (blue) as postsynaptic marker.

672 **Figure 6. Number of synapses**

673 **(a)** Development of the number of synapses per subgroup over time. (**b**) Group comparison of controls
674 vs PD patient cell-lines. (**c, d**) Representative fluorescence images for human autaptic neurons for each
675 subgroup at 4 WID. Synapse number were counted by colocalizing Synapsin1/2 puncta (presynaptic
676 marker, red) and Shank2 puncta (postsynaptic marker, blue) within proximity to dendrites (MAP2,
677 green). Control cell (**c**) and PD patient cell (**d**) with magnification of synapse: **i** MAP2, Synapsin 1/2,
678 Shank2, **ii** Synapsin 1/2, Shank2; **iii** Synapsin 1/2; **iv** Shank2.

679

Supplementary Figure 1:

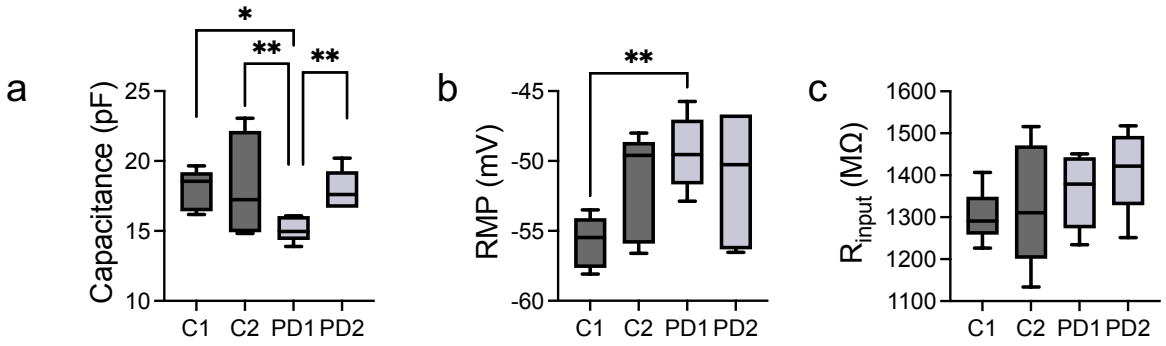

Supplementary Figure 2:

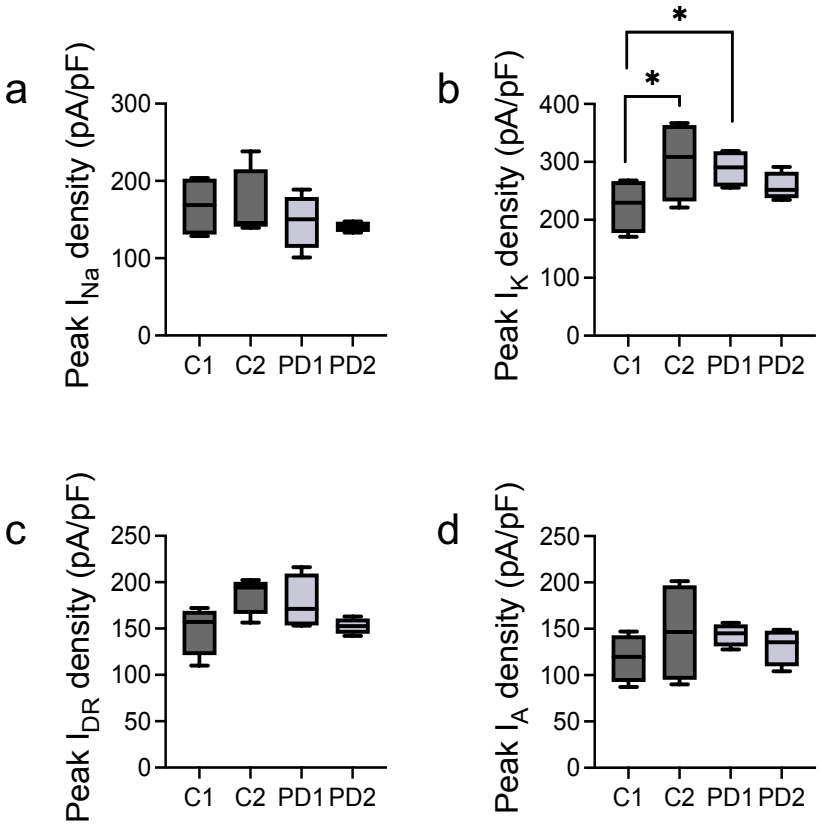

Supplementary Figure 3:

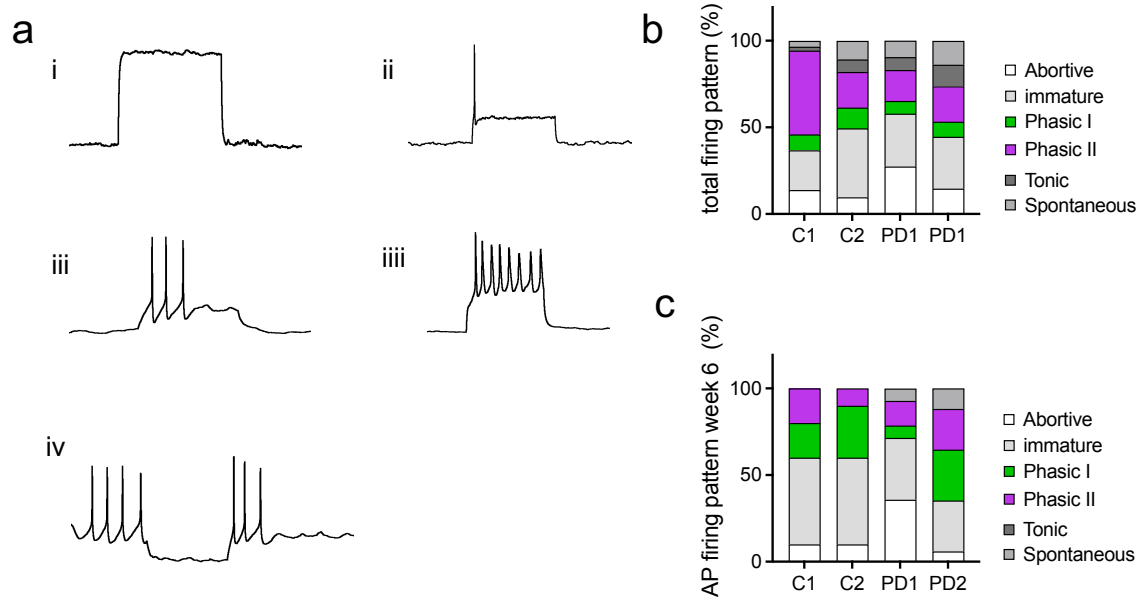

Supplementary Figure 4:

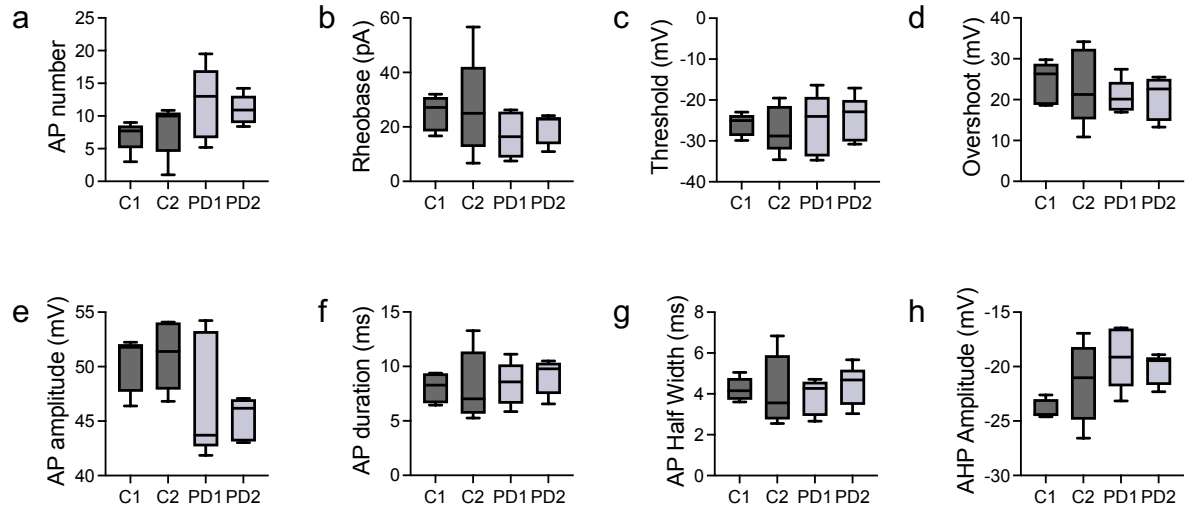

Supplementary Figure 5:

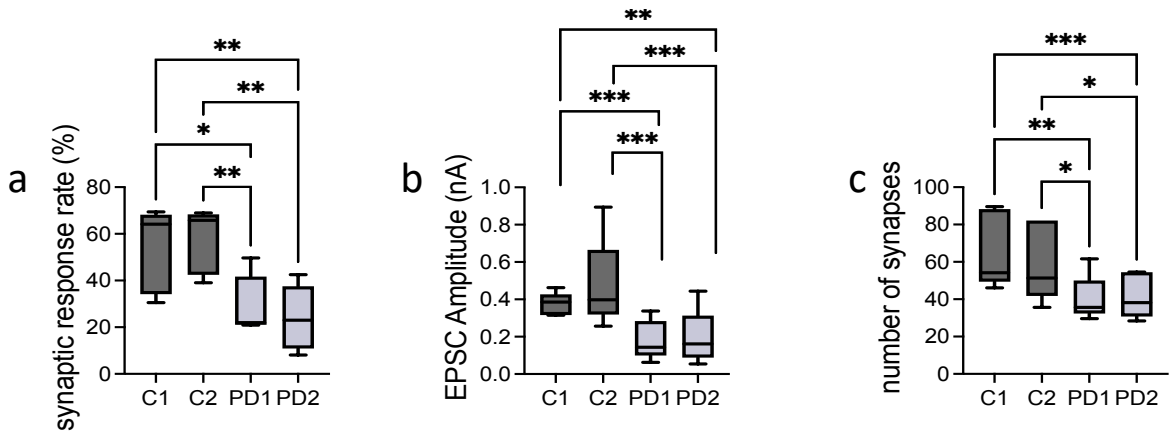

Supplementary Figure 6:

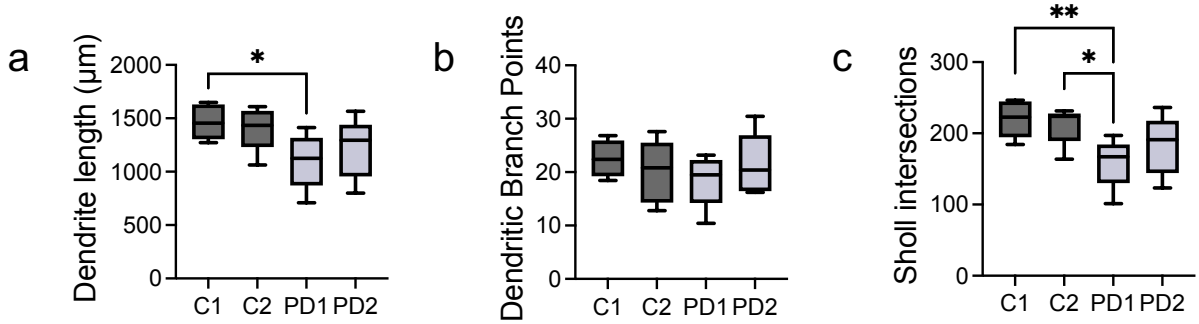

Supplementary Figure Legends

Supplementary Figure 1. Passive Membrane Properties

Graphs show subgroup comparison (C1, C2, PD1, PD2) of passive membrane properties. (**a**) Capacitance; 'subgroup' factor: p =0.0041, C1 vs. PD1: p =0.0465, C2 vs PD1: p =0.0096, PD1 vs PD2: p =0.0084, 2-way ANOVA with multiple comparison test Tukey). (**b**) RMP; 'subgroup' factor: p = 0.0128, C1 vs PD1: p = 0.0069, 2-way ANOVA with multiple comparison test Tukey. (**c)** R_{input}; there are no significant differences between subgroups.

Supplementary Figure 2. Voltage-gated Channels

Voltage-dependent Sodium and Potassium currents presented as peak densities per subgroups. **(a)** Graph for I_{Na} densities per subgroup; (**b-d**) Graph for total I_K (b), I_{DR} and I_A densities; Slight subgroup differences can be seen for peak I_K currents ('subgroup' factor: P= 0.0094, C1 vs C2: p = 0.019, C1 vs PD1: p = 0.0182, 2-way ANOVA with multiple comparison test Tukey).

Supplementary Figure 3. Action potential patterns

(a) Identified patterns of AP firing: abortive (**i**), phasic I (**ii**), phasic II (**iii**), tonic (**iiii**) and spontaneous (**iv**). Combined percentage of AP firing pattern per subgroup (**b**) and AP firing pattern of each subgroup at 6 WID (**c**). At 6 WID, no tonic and in controls no spontaneous firing cells were recorded.

Supplementary Figure 4. Active Membrane Properties; Parameters for action potential

(a-d) Subgroup comparison for various parameters of action potential shape. AP numbers (**a**) and AP-amplitudes (**e**) are slightly lower, respectively higher, in controls vs PD patient cell-lines.

Supplementary Figure 5. Synaptic response and number of synapses

Subgroup comparison of the proportion of neurons with AP-induced synaptic release, EPSC amplitude and number of synapses; (**a**) Synaptic response rate ('subgroup' factor: p = 0.0002, C1 vs PD1: p= 0.0229, C1 vs PD2: p = 0.0039, C2 vs PD1: p = 0.0071, C2 vs PD2: p = 0.0011, 2-way ANOVA followed by multiple comparison test Tukey), (**b**) EPSC amplitude ('subgroup' factor: p =<0.0001, C1 vs PD1: p = 0.0005, C1 vs PD2: p = 0.0013, C2 vs PD1: p = 0.0004, C2 vs PD2: p = 0.001, 2-way ANOVA with multiple comparison test Tukey). (**c**) Number of synapses ('subgroup' factor: p = <0.0001, C1 vs PD1: p = 0.0011, C1 vs PD2: p = 0.0009, C2 vs PD1: p = 0.0243, C2 vs PD2: p = 0.0264, 2-way ANOVA with multiple comparison test Tukey).

Supplementary Figure 6. Morphological Analysis with immunohistochemistry

Subgroup comparison for summed up dendrite length, number of dendritic branch points and Sholl intersections. Both PD patient cell-lines had shorter overall dendrite length (**a**) and average numbers of dendrites intersecting Sholl circles up to 200 μm distance from the soma (**c**) ('subgroup' factor: p = 0.0119, C1 vs PD1: p = 0.0192, **c**, subgroup' factor: p = 0.0051, C1 vs PD1: p = 0.0073, C2 vs PD1: p = 0.0355, 2-way ANOVA with multiple comparison test Tukey. Number of branchpoints did not differ clearly between subgroups (**b**).